Engineering Fracture Mechanics 232 (2020) 107041

Contents lists available at ScienceDirect

Engineering Fracture Mechanics

journal homepage: www.elsevier.com/locate/engfracmech

# Size effect in heterogeneous materials analyzed through a lattice discrete element method approach

Luis Eduardo Kosteski[a,*], Ignacio Iturrioz[b], Giuseppe Lacidogna[c], Alberto Carpinteri[d]

[a] PPEng, UNIPAMPA, Campus Alegrete, RS, Brazil
[b] PROMEC, UFRGS, Porto Alegre, RS, Brazil
[c] Department of Structural, Geotechnical and Building Engineering, Politecnico di Torino, Turin, Italy
[d] Department of Structural, Geotechnical and Building Engineering, Politecnico di Torino, Turin, Italy

ARTICLE INFO

*Keywords:*
Heterogeneous materials
Lattice Discrete Element Method
Size effect
Brittleness number

ABSTRACT

In the Lattice Discrete Element Method (LDEM), different types of mass are considered to be lumped at nodal points and linked by means of one-dimensional elements with arbitrary constitutive relations. In previous studies on the tensile fracture behavior of rock samples, it was verified that numerical predictions of fracture of non-homogeneous materials using LDEM models are feasible and yield results that are consistent with the experimental evidence available so far. In the present paper, a discussion of the results obtained with the LDEM is presented. A set of rock specimens of different sizes, subjected to monotonically increasing simple tensions, are simulated with LDEM. The results were analyzed from the perspective of the brittleness number, proposed by Alberto Carpinteri, to measure the brittleness level of the structure under study. The satisfactory correlation between the experimental results and LDEM results confirms the robustness of this method as a numerical tool to model fracture processes in quasi-brittle materials.

## 1. Introduction

In the literature, the scale effects were extensively studied to connect the fracture process zone with the specimen size, the pioneer works of Dugdale [1], Boyle [2], and Brown and Srawley [3] could be cited among others. More specifically, in the so-called quasi-brittle materials, such as concrete, this topic was also widely discussed. This kind of materials are characterized by a disordered microstructure, exhibits damage localization, and are unable to present plastic or hardening deformations, having a non-negligible fracture process zone compared to the structure size. Furthermore, it was observed that the structural behavior changes with the size of the analyzed specimen. Also the link between acoustic emission parameters and the ultimate strength was shown experimentally, among others by Mpalaskas [4,5], and this relation could be proposed for better understand the damage process in quasi-brittle materials.

Carpinteri [6–10] proposed dimensionless parameters: the brittleness numbers $s$ and $s_E$, to measure the structural brittleness that describes the susceptibility of cracks to propagate in unstable conditions. These numbers are related to the change of behavior with

* Corresponding author.
*E-mail addresses:* luiskosteski@unipampa.edu.br (L.E. Kosteski), ignacio@mecanica.ufrgs.br (I. Iturrioz), giuseppe.lacidogna@polito.it (G. Lacidogna), alberto.carpinteri@polito.it (A. Carpinteri).

https://doi.org/10.1016/j.engfracmech.2020.107041
Received 23 March 2020; Accepted 6 April 2020
Available online 15 April 2020

**Nomenclature**

| | |
|---|---|
| $A_i$ | cross-section area of the element to obtain the mechanical equivalence with the solid ($i = l$, longitudinal bars; $i = d$, diagonal bars) |
| $A_i^*$ | cross section to obtain the fracture equivalence with the solid material |
| $b$, $D$, $d$, $r$ | dimensions that define the specimens' geometries |
| $d_{eq}$ | characteristic length of the material |
| $E$, $\nu$ | elastic constant: Young's modulus and Poisson's ratio, respectively |
| ECL | Elemental Constitutive Law |
| $F$ | element axial force |
| $F(t)$, $P(t)$ | internal and external vector forces |
| $F_{max}$ | the peak force measured in each bar |
| $G_f$ | fracture energy |
| $K_c$ | the critical stress intensity factor |
| $L$ | length of the side of the cubic LDEM module |
| $L_{corr}$ | the correlation length |
| $L_d$ | length of the diagonal elements |
| LDEM | Lattice Discrete Element Method |
| $M$, $C$ | mass and damping matrices |
| $q$ | the critical crack size |
| $R$ | structure characteristic length |
| $s$, $s_E$ | both version of the brittleness numbers proposed by Carpinteri |
| $s_{LDEM}$ | Brittleness number computed in the context of LDEM |
| $w$ | displacement |
| $\ddot{x}$, $\dot{x}$ | nodal acceleration and velocity vectors |
| $Y$ | the shape coefficient |
| $Z$ | specimen length or span |
| $Z/R$ | the slender coefficient of the specimen |
| $\delta_c$, $\delta_{50}$, $\delta_u$ | characteristic displacements measured in the LDEM global stress-displacement responses |
| $\varepsilon_p$ | characteristic strain measured in each bar |
| $\varepsilon_r$ | failure strain measured in each bar |
| $\varepsilon_u$ | strain linked with $\sigma_p$ |
| ρ | specific mass |
| $\sigma$ | stress |
| $\sigma_p$ | global maximum strength |
| $\sigma_p^*$ | the stress that correspond with the $\varepsilon_p$ |
| $\mu(.)$, $CV(.)$ | mean value and variation coefficient |

the structural size and depend on the fracture energy and the yielding strength of the material as well as on the characteristic dimension of the structure:

$$s_E = \frac{G_f}{\sigma_p R};\ s = \frac{K_c}{\sigma_p R^{1/2}}. \tag{1}$$

In these expressions, $K_c$ is a measure of toughness, and $G_f$ is a mechanical characteristic of brittle materials called fracture energy, following the nomenclature used by Carpinteri in his Cohesive Crack Model presented in [9,11], $\sigma_p$ represent the

yielding or maximum stress, and $R$ constitutes the characteristic structural dimension that defines the specimen's size. If we consider that $K_c = (G_f E)^{0.5}$ and $\sigma_p = E\varepsilon_u$, then the equivalence between the two adimensional numbers is:

$$s_E = s^2 \varepsilon_u, \tag{2}$$

where $\varepsilon_u$ is the strain linked to $\sigma_p$.

Both nondimensional numbers have been used in several scientific papers in the last three decades [12–16, among others]. In Carpinteri [6,7], the characteristics of these parameters are presented in detail, and the recommendation that $s_E$ is more adequate to be used for brittle or quasi-brittle materials and $s$ for ductile materials is highlighted. In the present work, the $s$ instead of $s_E$ parameter was used to measure the change of global behavior in the specimens that were tested and consequently simulated by the model.

The numerical simulations of structures made of quasi-brittle materials have the implication that, in these materials, the characterization of the damage is often governed by more than one single crack. The studies of a set of small fractures interacting at different scale levels have great relevance when attempting to understand and simulate the behavior of these materials. As mentioned by Krajcinovic [17], accounting for each individual crack in the heterogeneous materials, assessing its influence on the structural response and ultimately on the structural failure, is not a task that can be approached by using conventional methods of analysis in solid mechanics. In this way, the methods, which are able to represent naturally the discontinuities, could be an alternative method of analysis. Among the non-conventional methods of continuous representation, Peridynamics is widely used. Such method belongs to the family of Discrete Element Methods. In this approach, the combination of nodes and associated discrete mass by means of an interaction law applied between neighbor nodes represents the continuum. The proposal carried out for the Peridynamics was used originally to represent the interaction force at the atomic level. Seleson [18] could be cited here as an example of this approach. Moreover, the same approach was also applied at large scale levels, all thanks to the pioneering work by Silling [19].

Another equivalent discrete approach is the Truss-like Discrete Element Method or Lattice Model. Various and relevant approaches study can be referred to; among others like the ones proposed by Schlangen and van Mier [20], Krajcinovic and Vujosevic [21], and, more recently, the works of Sagar and Prasad [22], Nagy et al. [23], and Rinaldi [24]. A review of the different versions of Discrete Element Method, including the Particle methods and Lattice approaches, is presented in Mastilovic and Rinaldi [25].

In the present paper, a version of the Lattice Discrete Element Method (LDEM) proposed by Riera [26] will be used. This method was developed originally to determine the dynamic response of plates and shells when failure occurs primarily by shear or tension under a shock wave caused by impact loading, as it is generally observed in concrete structures.

In the LDEM, the quantities of mass are considered lumped at nodal points and linked by means of one-dimensional elements with arbitrary constitutive relations. The satisfactory correlation between the experimental results and the LDEM predictions confirms the

robustness of this method as a numerical tool to model fracture processes in quasi-brittle materials. These findings were reported, among others, in a successful analysis of: shells subjected to impulsive loading [27–30], the fracture of elastic foundations on soft sand beds [31], the generation and propagation of an earthquake [32–35], the study of the scale effect in quasi-brittle materials [36–42]; the computation of fracture parameters in static and dynamic problems [43–46], the study of strength of brittle materials under high strain rates [47] and finally the acoustic emission events in quasi-brittle materials [34,35,48–50]. In Refs. [29–31,36,46,51], LDEM simulations were discussed in which quantitative comparison with experimental results in terms of global parameters, such as displacement versus loads or final configurations, are presented. The following section presents a brief description of the theoretical foundation of this method.

## 2. Lattice Discrete Element Method formulation

The Lattice Discrete Element Method (LDEM), used in the present work, represents the continuum by means of a 3D lattice, that is, a periodic spatial arrangement of bars with amounts of mass lumped at their ends. Fig. 1 shows the discretization strategy in which the stiffness of the LDEM elements, corresponding to an equivalent orthotropic linear elastic material, was obtained by Nayfeh and Hefzy [52]. The basic cubic module is built with twenty bars and nine nodes. Each node presents three degrees of freedom given by the spatial components of the displacement vector in the global reference system.

In case of an isotropic elastic material, the cross-sectional area $A_l$ of the longitudinal elements (those defining the edges of the module and those that are parallel to the edges connected to the node located at the center of the module) in the equivalent discrete model is:

$$A_l = \phi L^2, \tag{3}$$

where $L$ is the length of the side of the cubic module under consideration. The function $\phi = (9 + 8\delta)/(18 + 24\delta)$, where $\delta = 9\nu/(4 - 8\nu)$ accounts for the effect of the Poisson's ratio $\nu$ [49,30]. Similarly, the area $A_d$ of the diagonal elements is:

$$A_d = \phi {L_d}^2 = \frac{2}{\sqrt{3}}\delta\phi L^2, \tag{4}$$

were $L_d = \frac{2}{\sqrt{3}}L$ is the length of the diagonal elements. The coefficient $2/\sqrt{3}$ in Eq. (4) accounts for the difference in length between the longitudinal and the diagonal elements.

It is important to point out that, for $\nu = 0.25$, the correspondence between the equivalent discrete solid and the isotropic continuum is complete. On the other hand, for values of $\nu \neq 0.25$ discrepancies appear in the shear terms. These discrepancies are small and may be neglected in the range $0.20 \leq \nu \leq 0.30$. For values of $\nu$ outside this range, a different basic module should be used (see Ref. [52]). It is interesting to note that while no lattice model can exactly represent a locally isotropic continuum, it can also be argued that no perfect locally isotropic continuum exists in the physical world. Isotropy in solids is a bulk property that reflects the random distribution of the orientation of constituent elements. A comprehensive study on the effect of the LDEM lattice geometry on the value of the Poisson's ratio can be found in Ref. [53].

The equations of motion are obtained from equilibrium conditions of all forces acting on the nodal mass, resulting in a system of equations of the form:

$$M\ddot{x} + C\dot{x} + F(t) - P(t) = 0, \tag{5}$$

where $\ddot{x}$and $\dot{x}$ are, respectively, the nodal acceleration and velocity vectors; $M$ and $C$ are the mass and damping matrices, respectively, and the vectors $F(t)$ and $P(t)$ convey the nodal internal and external forces. Since $M$ and $C$ are diagonal, the equations in Eq. (5) are not coupled, and they can be easily integrated in the time domain using an explicit finite difference scheme.

It is worth noting that, since the nodal coordinates are updated at each time step, large displacements are accounted for naturally.

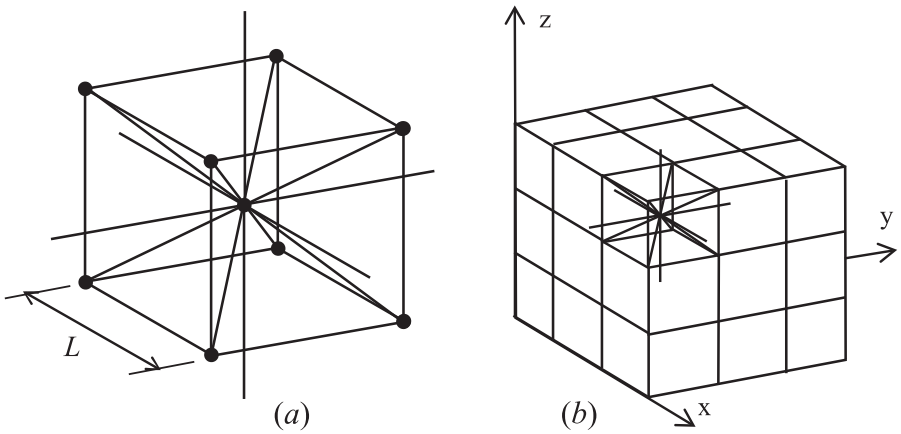


**Fig. 1.** LDEM discretization strategy: (a) basic cubic module, (b) generation of the prismatic body.

The convergence of LDEM solutions in linear elasticity and elastic instability problems was verified by [32], among others.

The irreversible effects of crack nucleation and propagation that occur in brittle or quasi-brittle materials were taken into account by [54], and more recently by [45], through the introduction of a non-linear constitutive model that reduces the element load carrying capacity. More details of this implementation can be found in [43–46,54], among others.

Based on Hillerborg's theory [55], the bilinear model for quasi-brittle materials used in this work is shown in Fig. 2. In case of tensile loads, the area under the force - strain curve (the area of the *OAB* triangle in Fig. 2) is the energy density necessary to fracture the area of element influence, the fracture energy. Thus, for a given point *P* on the force - strain curve, the area of the *OPC* triangle represents the reversible elastic energy density stored in the element, while the area of the *OAP* triangle is the dissipated fracture energy density. One element fails and loses its load carrying capacity when the dissipated energy density equals the fracture energy.

In the case of compressive loads, the material behaves in a linear elastic manner. In this way, the failure in the compression is induced by indirect traction. In quasi-brittle materials, this assumption is reasonable because its ultimate strength in compression is usually five to ten times larger than that in tension [56].

In the constitutive model presented in Fig. 2, $F$ is the element axial force, and $A_i$ the cross-section area of the element, depending whether longitudinal or diagonal element is considered, as in Eqs. (3) and (4). In this model, the fracture energy per unit area coincides with the material fracture energy, $G_f$.

The so called critical strain $\varepsilon_{p,}$ as illustrated in Fig. 2, is the maximum strain before damage initiation. The critical strain is a micro-parameter, that is, a parameter that governs the constitutive law at the elemental level. The *limit strain* $\varepsilon_r$ is the strain value for which the elements lose its load carrying capacity (point B in Fig. 2). The limit strain is much greater than or equal to the critical strain. This value is calculated to satisfy the fact that the dissipated energy density released when the element fail must be equal to the multiplication of the equivalent fracture area of the element, $A_i^*$, times the fracture energy, $G_f$, divided by the element length, $L$, that is:

$$\int_0^{\varepsilon_r} F(\varepsilon)d\varepsilon = \frac{G_f A_i^*}{L_i}. \tag{6}$$

The index $i$ in the expression indicates it either refers to longitudinal or the diagonal elements.

The area below the bilinear model is $\varepsilon_r \varepsilon_p E A_i/2$, then, the final strain defined for the element $\varepsilon_r$, illustrated in the Fig. 2, is designated as:

$$\varepsilon_r = \frac{G_f}{\varepsilon_p E}\left(\frac{A_i^*}{A_i}\right)\left(\frac{2}{L_i}\right), \tag{7}$$

$A_i^*$denotes the equivalent fracture area of each element defined in order to satisfy the condition that the energy dissipated by the fracture of the continuum and by its discrete representation are equal, $A_i^* = \frac{3}{22}L_i^2$. This deduction can be found in [45]. It should be noted that $\varepsilon_r$ depends on the material properties and on the level of discretization.

Young's modulus$E$, the stress intensity factor $K_c$ and the critical stress $\sigma_p$ are related by the classical fracture mechanic expression [57] given below:

$$K_c = \sigma_p Y\sqrt{\pi q}, \tag{8}$$

in which $Y$ is a parameter that accounts for the influence of the boundary conditions and the orientation of the critical crack size $q$. If it is assumed that the behavior up to the beginning of the rupture is linear, then $\sigma_p^* = E\varepsilon_p$ and, recalling the equivalence between $K_c$ and the fracture energy $G_f$, we obtain the expression:

$$\sqrt{G_f E} = E\varepsilon_p Y\sqrt{\pi q}. \tag{9}$$

This assumption is very important for this development because the tension obtained ($\sigma_p^* = E\varepsilon_p$) is not the global maximum

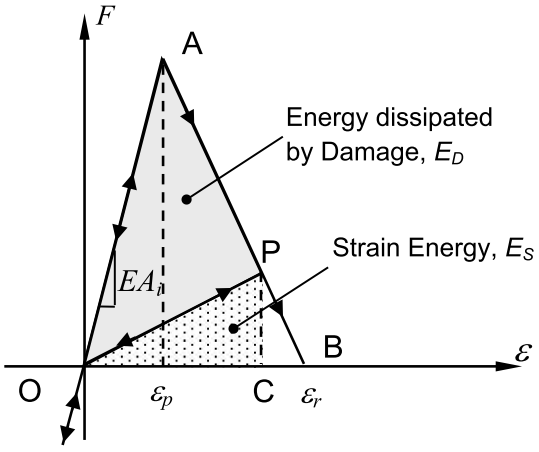


**Fig. 2.** Bilinear constitutive model with material damage.

strength $\sigma_p$, as defined in Eq. (1), but instead, is a local or elemental maximum.

In order to simplify Eq. (9), an equivalent length $d_{eq}$is defined as follows:

$$d_{eq} = q\pi Y^2. \tag{10}$$

Substituting Eq. (9) in (10), then:

$$d_{eq} = \frac{G_f}{(\varepsilon_p)^2 E} \tag{11}$$

Eq. (11) indicates that $d_{eq}$ may be regarded as a material property, since it does not depend on the discretization level, representing in fact a *characteristic length of the material* (similar as the width of the plasticity region in the crack tip in the Dugdale model).

It also is possible to isolate $\varepsilon_p$ from the Eq. (11) to obtain:

$$\varepsilon_p = \sqrt{\frac{G_f}{d_{eq} E}}, \tag{12}$$

and replacing (11) in $\varepsilon_r$ Eq. (7) it is found:

$$\varepsilon_r = \varepsilon_p d_{eq} \left(\frac{A_i^*}{A_i}\right)\left(\frac{2}{L_i}\right), \tag{13}$$

Eq. (12) shows that maintaining $E$ and $G_f$constant, when the $d_{eq}$ increases, a more ductile behavior is expected. The area below the elemental constitutive relation (see Fig. 2) is linked to $G_f$, then, if this parameter remains constant, the decrease of $\varepsilon_p$ has to be compensated by increasing the value of $\varepsilon_r$to maintain the area below the curve.

When $\varepsilon_p$ is equal to $\varepsilon_r$, the minimum area of bilinear constitutive model is obtained, that is, the limit relation between the equivalent length and the element length, for longitudinal elements, is found to be$d_{eq} \geq \frac{15}{22}L$. In some way, from the Eq. (13) it is possible to say that$\varepsilon_r/\varepsilon_p \propto d_{eq}/L$, that is, $d_{eq}/L$ is related to the bilinear constitutive model. If the constitutive model is "brittle" ($\varepsilon_r$ next to $\varepsilon_p$), $d_{eq}/L$ will be small, however, if the constitutive model is "ductile" ($\varepsilon_r$ much larger than $\varepsilon_p$) $d_{eq}/L$ will be higher.

It can be noticed that a characteristic length as material parameter is also discussed in another version of the discrete element method called Peridynamics, proposed by Silling et al. [58]. In this method, there is a set of nodes where the mass are discretized and linked with bars, moreover, the level of neighboring among nodes is given by a material parameter called horizon. This parameter depends on the discretization level used to define the quantity of nodes linked to one and another. The horizon physical meaning is analogous to the meaning of the $d_{eq}$ in the version of the Discrete Element Method used in the present work.

Taylor [59] considers that a breaking criterion is fulfilled when a dominium portion, defined by a characteristic dimension, reaches the critical level of stress. In this approach, both parameters are considered as material parameters. The link between the characteristic distance of this author and the $d_{eq}$ is evident.

The randomness of the model is introduced considering $G_f$ as a random field with a Weibull density function characterized by its mean value $\mu(G_f)$ and variation coefficient $CV(G_f)$. Moreover, it is necessary to consider the spatial correlation function of this random parameter. How to consider the random nature in the model could be explained in [30,60].

In the model here implemented, the random values of $G_f$ assigned to every element have statistical independence, that is, the random properties of one element do not depend on the properties of the other neighboring elements. This assumption is equivalent to consider that the correlation length is $L_{corr} = 0.3L$. Notice that when randomness is introduced in $G_f$, indirectly randomness is also introduced in $\varepsilon_p$ (see Eq. (12)). In this way, the maximum strength of an element $F_{max} = EA_i\varepsilon_p$, which is directly related to point A in Fig. 2, is also random. The axial stress of the element will be: $\sigma_p^* = E\varepsilon_p$. Another alternative to introduce the random nature in the model is to consider geometric perturbation in the mesh, about this aspect see [61]. More detail about the LDEM formulation can be found in Ref. [50].

Below, several points are explained to clarify the meaning of the parameters used in the definition for the constitutive law of the LDEM model:

(i) The concept of the brittleness number $s$ in the context of LDEM is introduced with the aim of showing evidence of the physical meaning of the parameter $d_{eq}$ previously defined.

If we rewrite the Eq. (1) that introduces the *brittleness number* $s$ proposed by Carpinteri [6], we consider that $\sigma_p = \sigma_p^*$ and recalling the equivalence between $K_c$ and the fracture energy $G_f$, the expression of $s$ in the context of the LDEM formulation will be:

$$s_{LDEM} = \frac{K_c}{\sigma_p^* R^{1/2}} = \frac{\sqrt{G_f E}}{E\varepsilon_p R^{1/2}} = \sqrt{\frac{d_{eq}}{R}}. \tag{14}$$

From this expression it can be interpreted that, if a crack of a size $> d_{eq}$ appears during the damage process in a structure with a characteristic dimension $R$, it will propagate in an unstable form, suggesting a brittle global structural behavior. However, this situation will only be possible if $d_{eq}$is lower than $R$. If this condition is not fulfilled, it will not be possible to have a crack with a dimension similar to $d_{eq}$, because there is not enough space in the structure for crack propagation. In the latter situation, the structure will have a ductile behavior during its damage process. The structure boundary condition influences this relation but it does not

change the general tendency.

The ratio between Eqs. (1) and (14) allows writing the relationship between the traditional expression of the brittleness $s$ with its definition in the context of LDEM. As it was previously emphasized, the difference resides in the definition of $\sigma_p$: in the classical expression of $s$, $\sigma_p$ is the stress value in which the material collapses, while in the $s_{LDEM}$ definition, $\sigma_p = \sigma_p^*$ is the axial stress of the elements. The ratio $s/s_{LDEM}$ is a function of the statistical and spatial distribution of the random field that characterizes$G_f$, and the shape of the elemental constitutive law used. At the end of the present work, a further comment about this ratio is provided.

(ii) In contrast to the usual practice used in the Finite Element Method, the constitutive relationship in the LDEM is not only a function of the material properties. The LDEM model considers the following macroscopic parameters: the elastic modulus $E$, the fracture energy $G_f$, and the characteristic length $d_{eq}$. With these three parameters using Eq. (12), the critical strain$\varepsilon_p$, where the bar force reaches its maximum value is computed (see Fig. 2). Multiplying $E$ by the Eqs. (3) and (4) the linear pre-peak relation in the elemental constitutive law (ECL), defined by $EA_i$, is indicated in Fig. 2. The fracture energy $G_f$ directly influences in the area below the ECL, as it is indicated in Eq. (6). Furthermore, using Eq. (13) as illustrated in Fig. 2, the characteristic length of the material, $d_{eq}$, defines the post-peak branch in the ECL by means of the local parameter $\varepsilon_r$. Notice that not only$\varepsilon_r$, but also $EA_i$ depend on the discretization level.

(iii) Another interesting feature of the method is that, although it uses a scalar damage law to describe the uniaxial behavior of the elements, involves a global model that takes into account of the anisotropic damage. This is because, when the uniaxial bars, oriented in different directions, are damaged they modify their axial stiffness, allowing to represent an anisotropic global behavior.

## 3. Experimental background

The results obtained by Carpinteri and Ferro [62,63], van Vliet [64] as well as van Vliet and van Mier [65], all of whom have studied the scale effects on tensile strength of concrete and rock, are used to explore the link between the brittleness number, $s$, proposed by Carpinteri [6,7] and the global behavior obtained in the cited cases that could be classified as ductile or brittle. Experimental results obtained by the authors over expanded polystyrene samples are also described and analyzed.

### 3.1. Carpinteri and Ferro results

Carpinteri and Ferro [62,63] and Carpinteri and Maradei [66] carried out two sets of tests with specimens of several sizes. The Young's Modulus was measured from the global stress versus strain curves, at around 35GPa for the two sets. The material parameters and the brittleness number values $s$, computed using Eq. (1), are presented in Table 1. The characteristic dimension $R$ was considered in the present case as the dimension of the specimen neck, $d$.

In both series, the specimen with characteristic size $d$ smaller than 100 mm showed a ductile behavior, whereas specimens with $d$ larger than 200 mm showed a quasi-brittle behavior. In both sets of results $s < 1.4$ indicates a quasi-brittle global behavior

### 3.2. van Vliet and van Mier's results

van Vliet [64] performed three sets of tests of specimens using different dimensions, as is shown in Fig. 3. The first set was conducted by using concrete stored in the laboratory in a dry environment, called the DRY set. The second set also was with concrete, however stored in a climate room, called the WET series. Finally, the third set of specimens consists of Felser sandstone specimens called FELSER.

For the calculus of the brittle number, the fracture energy $G_f$ measured extrapolating the stress opening curve ($\sigma$-$w$) was used. The material parameters and the $s$ values computed are presented in Table 2. In the present cases, the characteristic dimension $R$ to compute the brittleness number $s$ with the Eq. (1) is $0.6D$, the specimen neck, as could be appreciated in Fig. 3.

For all the van Vliet experiments, represented in Table 2, it is possible to observe an apparent change in the global behavior for specimen with brittle number $s$ near to 1.5. For $s$ values lower than 1.6, specimen F ($s = 1.34$) for the DRY set, specimen D ($s = 1.57$) for the Wet set and specimens D ($s = 1.48$), E ($s = 1.07$) and F ($s = 0.74$) for the FELSER set, the global response seems to be brittle. Finally, for $s$ values higher than 1.6, a clearly ductile global response is observed.

In fact, it is possible to consider that with $s$ between 2 and 1 we are in a transition zone, and a very clear brittle behavior could be defined when $s$ is lower than 1, as seen for the F($s = 0.74$) specimen in the FELSER set.

### 3.3. Expanded polystyrene experimental results

In the following section, a set of tests carried out by the authors on expanded polystyrene are presented. The material was submitted to direct tensile stress using specimens with the same geometry, but different sizes compared to the ones used by Van Vliet [64]. The tests were carried out in a Universal Machine Test Shimadzu AGS - X 5 kN in the Federal University of Pampa - Brazil.

In Table 3 the dimensions of the body tests called A, B, C and D are presented. Four tests were conducted for each configuration. For all the four specimen geometries, the thickness was always 9 mm. The specimens were fixed at the ends, as illustrated in Table 3 by applying the prescribed displacement at the top end at a constant displacement rate of 0.0333 mm/min.

Fracture energy $G_f$ equal to 25 N/m, value also adopted by Colpo *et al.* [42], was used for the calculus of the brittleness number by

using Eq. (1). These results are presented in Table 4. As done in previous tests, the specimen characteristic length $R$ was considered to be equal to the neck specimen, $0.6D$.

A similar tendency, to what was observed in previous cases, was also appreciated in the results obtained using expanded polystyrene. When the $s$ value is lower than 1, the global stress curve clearly shows a brittle behavior, and when the results of $s$ are between the interval 2.0 and 1.0, a transition behavior is observed.

With the aim of categorizing the global behaviors in all the tests carried out, a typical brittle global response it is considered when:

(a) considering tests under controlled displacement, after reaching the peak load, the global displacement is smaller than that corresponding to the peak load. As in the case of the (F) specimens of the FELSER sandstone set presented in Table 2;
(b) considering tests under force control, after reaching the peak load, the behavior is characterized by a clear jump in the load, without any significant softening branch. The specimen (D), presented in Table 4, is an example of this second case.

On the other hand, a typical ductile global behavior is considered when the global post-peak displacement is higher displacement corresponding to the peak load. The Felser tests from (A) to (C), presented in Table 2, are clear examples of this kind of global behavior.

When it is not possible to define a clear brittle, or ductile behavior, we consider this case as a global transition behavior, see, for example, specimen (A) of the Polystyrene specimens presented in Table 4.

It is important to highlight here that, in Carpinteri [6,7], the author reaches the conclusion that, for specimens subjected to tension or compression, the following equation

$$\frac{s_E}{\left(\frac{Z}{R}\right)\varepsilon_u} \leq \frac{1}{2}, \tag{15}$$

defines the condition for Snap-Back instability that governs the global mechanical behavior. In the Eq. (15), $Z$ is the specimen length or span and $Z/R$ represents the slenderness. For the cases studied in the present work, $Z/R$ is always considered close to 1. Remembering the equivalence given between $s_E$ and $s$ presented in Eq. (2), Eq. (15) could be rewritten in terms of $s$ as $s^2 \leq 1/2$, i.e. $s \leq 1/\sqrt{2} \sim 0.7$, a result that could be considered as a lower bound for the numerical results presented in the following section.

However, in the three experimental results presented, the shape of the specimens considered is not prismatic. Therefore, the difference in shape could explain that, in the described conditions, the transition to the brittle behavior seems to be defined by $s \leq 1$ instead of $s \leq 0.7$. The extension of the present study with the aim of verifying the influence of the slenderness, other geometric characteristics as well as other boundary conditions will be the focus of future works.

**Table 1**
Material parameters, the brittleness number computed and the curves used as sources of information for the experimental sets 1 and 2 presented by Carpinteri and Ferro [62,63]. ($E$ = 35 GPa).

| $d$ [mm] | $\sigma_p$ [MPa] | $G_f$ [N/m] | $s$ | Experimental Results | Specimen Geometry |
|---|---|---|---|---|---|
| Set 1 | | | | | |
| 50 | 4.25 | 83 | 1.79 | 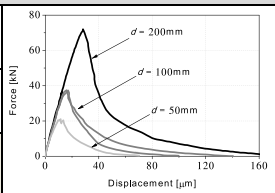 | 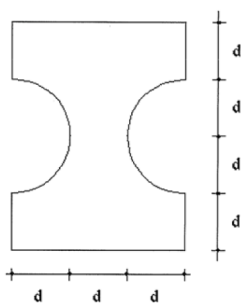 |
| 100 | 3.78 | 102 | 1.58 | | |
| 200 | 3.64 | 142 | 1.37 | | |
| Set 2 | | | | | |
| 25 | 4.79 | 147 | 2.99 | 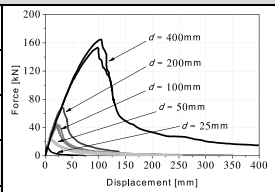 | |
| 50 | 4.56 | 257 | 2.94 | | |
| 100 | 4.37 | 236 | 2.08 | | |
| 200 | 3.80 | 158 | 1.38 | | |
| 400 | 3.72 | 286 | 1.34 | | |

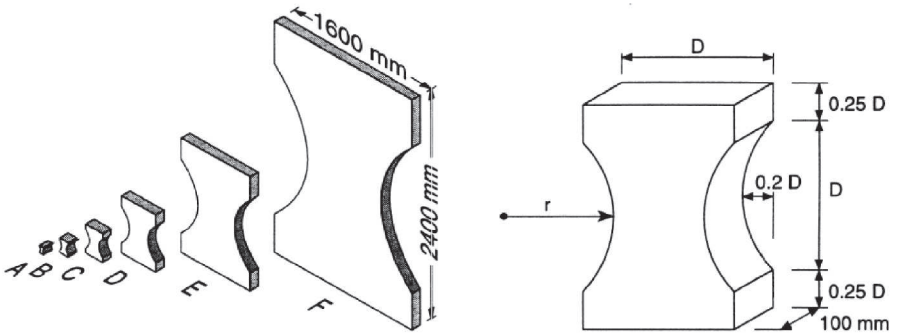


| Type | A | B | C | D | E | F |
|---|---|---|---|---|---|---|
| $D$ [mm] | 50 | 100 | 200 | 400 | 800 | 1600 |
| $r$ [mm] | 36.25 | 72.5 | 145 | 290 | 580 | 1160 |

**Fig. 3.** Specimen shape and dimensions for van Vliet [64] adopted size range.

**Table 2**
Material parameters and brittleness number computed for the van Vliet [64] specimens.

| Type | $\sigma_p$ [MPa] | $G_f$ [N/m] | $E$ [GPa] | $s$ | |
|---|---|---|---|---|---|
| DRY set | | | | | |
| A | 2.54 | 97.0 | 88.42 | 6.66 | 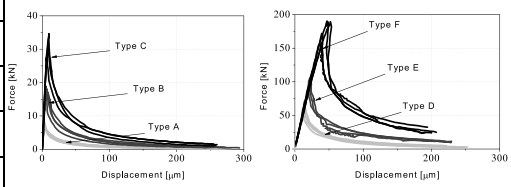 |
| B | 2.97 | 125.7 | 38.5 | 3.02 | |
| C | 2,75 | 124.2 | 39.41 | 2.32 | |
| D | 2.30 | 125.2 | 42.80 | 2.05 | |
| E | 2.07 | 142.3 | 38.25 | 1.63 | |
| F | 1.86 | 141.1 | 42.55 | 1.34 | |
| WET set | | | | | |
| A | 2.17 | 91.1 | 40.48 | 5.11 | 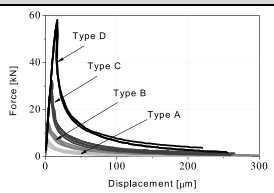 |
| B | 2.23 | 99.6 | 39.80 | 3.64 | |
| C | 2.48 | 88.9 | 42.38 | 2.26 | |
| D | 2.37 | 100.4 | 33.25 | 1.57 | |
| FELSER sandstone set | | | | | |
| A | 0.82 | 76.7 | 4.75 | 4.25 | 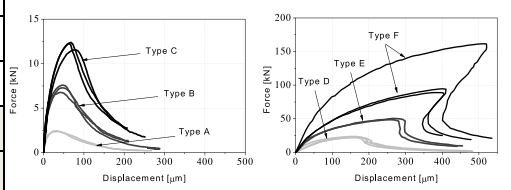 |
| B | 1.22 | 111.3 | 7.90 | 3.14 | |
| C | 1.01 | 93.8 | 6.87 | 2.29 | |
| D | 0.96 | 135.1 | 3.60 | 1.48 | |
| E | 1.30 | 143.9 | 6.50 | 1.07 | |
| F | 1.20 | 93.2 | 8.23 | 0.74 | |

**Table 3**
Body test dimensions.

| Type | A | B | C | D |
|---|---|---|---|---|
| $D$ [mm] | 10 | 20 | 30 | 45 |
| $r$ [mm] | 7.25 | 14.5 | 21.75 | 32.63 |
| |  | 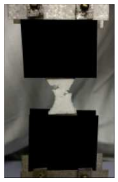 |  |  |

**Table 4**
The brittleness number computed for the set of test carried out over expanded polystyrene specimens.

| Type | $\sigma_p$ [MPa] | CV [%] | $E$ [N/mm$^2$] | CV [%] | $s$ | |
|---|---|---|---|---|---|---|
| A | 0.049 | 21.4 | 0.89 | 12.1 | 1.24 | 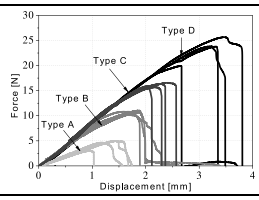 |
| B | 0.059 | 3.4 | 1.73 | 8.4 | 1.02 | |
| C | 0.060 | 2.5 | 2.01 | 12.8 | 0.88 | |
| D | 0.058 | 10.4 | 2.21 | 9.3 | 0.78 | |



## 4. LDEM simulations: Rock specimens with different sizes subjected to uniaxial tensile stress

### 4.1. Model description

A specimen group of heterogeneous material was simulated being fixed at their lower face and subjected to monotonically increasing displacements at the nodes on their upper faces. In all cases, nodal displacements in the normal direction to the middle surface were restrained in order to simulate plane strain conditions. The specimens were analyzed up to the complete failure. The specimen side $b$ ranges between an interval of 0.05 and 3.50 m. The smallest LDEM array that leads to satisfactory results consists of $10 \times 10 \times 1$ cubic modules with 1026 DOF which were used for the smallest (0.05 m) model. Whereas the 3.50 m model consists of $700 \times 700 \times 1$ cubic modules with 1,472,802 DOF, thus, constituting the largest specimen used in this study. Table 5 shows the basic dimensions of the samples, while Table 6 indicates the relevant material properties.

It is important to note that in the simulations, the expected value of the fracture energy, $\mu(G_f)$, was considered as a mean value for all the sizes being simulated, instead of considering it as a variable with the size scale.

The layout of the specimens showing their relative size and boundary conditions is shown in Fig. 4. It should be noticed that the fracture energy $G_f$ is modelled as a random field using the properties indicated in Table 6. The probability distribution of $G_f$ was considered as a Weibull function with a correlation length equal to $L_{corr} = 0.3L$, which is related to the material microstructure. As the material properties are associated with a statistical distribution, each simulation leads to a different strength and a different stress–strain curve. For this reason, four simulations were carried out for each size specimen in order to obtain representative results for each size specimen. As explained before, the correlation length used in this work is small, then the random values of $G_f$ assigned to every bar are statistically independent, that is, the properties of one bar do not depend on the properties of the neighbor ones.

### 4.2. Results

One representative sample of the final simulated configuration for each size considered in the study is shown in Fig. 5, in which the colors cyan, orange, and red represent undamaged, damaged, and totally broken (failed) elements, respectively. The sizes of the specimens are indicated in Fig. 4.

The influence of the mesh discretization is studied in Refs. [46,60], moreover, in the simulations presented here, the discretization level is similar. In addition, in Ref. [67] was verified that the influence of the mesh rotation is marginal (less than 5%) in terms of global results and fracture configurations.

The resulting stress displacement curves for all simulations of the $b = 0.20$ m specimens, as well as the average curve, are shown

in Fig. 6. In this figure, the main parameters that characterize the stress displacement curves are represented, in which $\sigma_p$ denotes the ultimate or maximum global stress, $\delta_c$ represents the critical displacement, or displacement related to ultimate stress, and $\delta_u$ represents the ultimate displacement or the displacement at the point where the strength is totally exhausted which has been defined for practical purposes as the displacement when the stress decreases below 2% of the maximum stress, $\sigma_p$. This notation is applicable without any restriction to specimens with sides smaller than 0.4 m. For specimens with $b$ equal to 0.4 m or larger, failure occurs in a brittle manner and the ultimate displacement $\delta_u$ cannot be distinguished from the critical displacement $\delta_c$. Fig. 6 also shows the displacement defined as $\delta_{50}$, that is, the displacement related to 50% of the rupture stress.

In Fig. 7(a) the global displacement versus mean stress curve for all the sizes simulated with LDEM are shown. In Fig. 7(b) the same results are presented considering the global displacement in a Log scale. In these figures, it is possible to see how the curves trend changes: specimens smaller than 0.25 m show a ductile behavior (black lines), specimens larger than 0.75 m present a brittle behavior (gray lines), whereas specimen sizes between 0.25 and 0.75 m show a transition between ductile and brittle behavior (red lines).

The simulations resulted in different fracture patterns that in some cases produced one, two or more cracks. It is worth noticing that the auto-similar configuration was used throughout this work. For this reason, simulations, in which only one macro-crack propagate, were considered. As it can be seen in Fig. 5, b = 3.5 m, there is more than one crack in the final configuration, but the other cracks or its bifurcation become stable and do not propagate to broke the specimen. When more than one crack propagates, the stress–strain curves present a different morphology.

As shown in Fig. 6, it is possible to specify the stress - displacement curves through characteristic values without losing essential information. Table 7 lists the correspondent characteristic mean values of the stress-displacement curves by increasing the specimens' size.

Table 7 also presents the Carpinteri's brittleness number $s$ obtained by Eq. (1), assuming that $R = b$ the size of the specimen, and $E$ and $G_f$ the simulations parameters presented in Table 6.

By comparing the stress-displacement curves presented in Fig. 7, it is possible to identify two limits, i.e., brittleness numbers that define changes in the specimen behavior: $s_{ub} \cong 1.5$ (upper bound), and $s_{lb} \cong 0.7$ (lower bound). Ductile behavior is expected for $s > s_{ub}$, brittle behavior for $s_{lb} < 0.7$, and transitional behavior when $s_{lb} < s < s_{ub}$.

The experimental and numerical results in terms of the brittleness number $s$, and global behavior (brittle-ductile transition), are shown in Fig. 8. A global brittle behavior is considered if $s$ is smaller than 0.7, a ductile one if $s$ is higher than 1.5. A transition can be considered if $s$ is comprised in the interval [0.7, 1.5]. It should be noted that $s < 0.7$ is a lower bound, but tests with brittle global behavior can occur with values above this limit. Furthermore, the ductile transition limit $s > 1.5$ shows a certain level of dispersion. The specimen shape and the influence of boundary conditions could be responsible for this dispersion. But despite this behavior, the limits $s < 0.7$ and $s > 1.5$ identify that the typical brittle-ductile transition take place in the specimens.

In Fig. 9(a), the size effect in the mean ultimate stress is presented, and in Fig. 9(b) the mean critical and ultimate displacement is also plotted. In both cases, the log scales are used to facilitate the result interpretation. A bar with ± 2 standard deviation is included in the plots and between this bar 95% of the values obtained in the simulation are contained.

In Fig. 9(a), it is clear that the size effect in the global ultimate stress is practically null. This effect could be seen in the values presented in Table 7. The difference between the maximum and minimum values of mean global stress is 1.23% and the variation coefficients do not exceed 1.64%. The sensitivity of the global parameters with the size effect depends on several factors, such as the boundary conditions, and the random nature of the material input data. In Rios and Riera [36] experimental tests with different geometries and boundary conditions were simulated with LDEM, and the values of strength and its variability are reached with success.

On the other hand, in Fig. 9(b) the specimen behavior changes in shape clearly for $b = 0.4$ m; this result is compatible with the limits indicated in Fig. 7 and in Table 7.

A new parameter was defined to take into account the shape of the global stress versus displacement curve, or force versus displacement. The parameter proposed was the ratio $\delta_{50}/\delta_c$, between the displacement $\delta_{50}$, when 50% of the rupture stress was reached, over the displacement $\delta_c$, when the ultimate stress occurred. Thus, when a value of $\delta_{50}/\delta_c$ is close to 1.0, a brittle behavior with unstable propagation is expected. $\delta_{50}/\delta_c > 1$ means that the specimen will present a ductile behavior and a stable rupture is foreseen.

In Fig. 10, the relation between the ratio $\delta_{50}/\delta_c$ and the brittleness number $s$ is shown for the experimental and numerical results presented in this work. In this plot, it clearly appears that for values of $s$ higher than 1.5, ratios of $\delta_{50}/\delta_c$ higher than 1.4 are obtained, therefore, indicating an evident ductile behavior for the specimen.

When $s$ presents values between 0.7 and 1.5, the ratio $\delta_{50}/\delta_c$ varies between 1.4 and 1; in these cases the specimens present a transitional ductile-to- brittle behavior.

Finally, when $s$ is lower than 0.7, the ratio $\delta_{50}/\delta_c$ will present values lower than 1.0, thus, characterizing a clear brittle behavior. It

**Table 5**
The dimensions of the LDEM models studied.

| Specimen | 1 | 2 | 3 | 4 | 5 | 6 | 7 | 8 | 9 | 10 | 11 | 12 | 13 |
|---|---|---|---|---|---|---|---|---|---|---|---|---|---|
| $b$ (m) | 0.05 | 0.075 | 0.10 | 0.15 | 0.20 | 0.25 | 0.30 | 0.40 | 0.50 | 0.75 | 1.00 | 1.50 | 3.50 |
| Cells | 10 | 15 | 20 | 30 | 40 | 50 | 60 | 80 | 100 | 150 | 200 | 300 | 700 |

**Table 6**
Relevant rock (granite) material properties and LDEM parameters.

| **Material Properties** | **Value** |
|---|---|
| $E$ (Young's modulus) | 75 GPa |
| ρ (specific mass) | 2700 kg/m$^3$ |
| $\nu$ (Poisson coefficient) | 0.25 |
| **LDEM Properties** | **Value** |
| $L$ (basic modulus length) | 0.005 m |
| $d_{eq}$ | 1.465 m |
| $\mu(G_f)$(Expected value of fracture energy) | 1300 N/m |
| CV($G_f$) (coefficient of variation of $G_f$) | 40% |

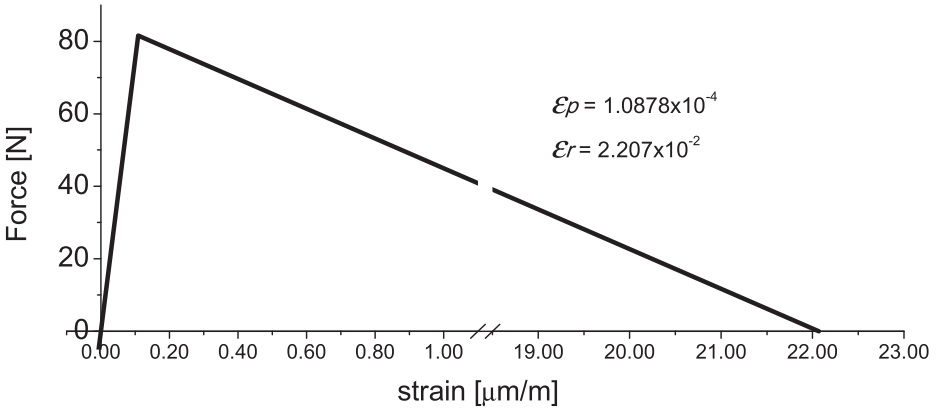


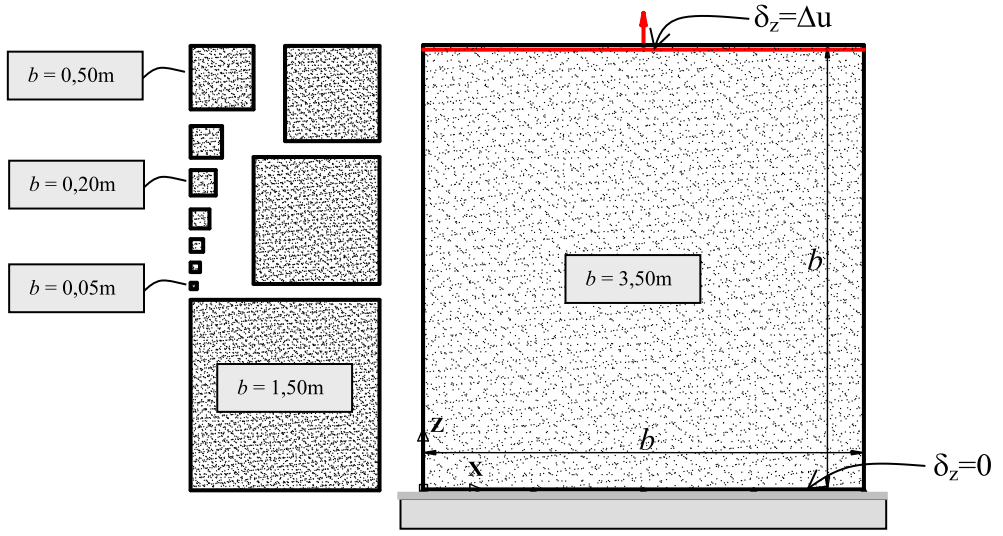


**Fig. 4.** Relative size of the specimens and boundary conditions considered.

was noticed that, in this region, for several cases, the ratio $\delta_{50}/\delta_c$ appears to be equal to 1.0. This is the typical value when the simulation is performed in a controlled displacement, when the specimen breaks in an unstable way and the snap-back branch of the curve is not captured. It is evident in the results of the Felser sandstone sets that, for specimens with $s < 1.0$, a special displacement control allows to capture the snap-back branch during the softening.

Finally, the ratio between the Carpinteri's number $s$ computed for the specimen and the $s_{LDEM}$ parameter computed in the context of the method is presented hereafter. In Fig. 10, the ratio $s/s_{LDEM}$ was plotted against the ratio $d_{eq}/L$, the latter measuring the relationship between the material length $d_{eq}$, that is a characteristic length of the material, as defined in section 2, and the size of the element that define the level of discretization used in the model.

In Fig. 11, it is possible to verify in which way the variability of the fracture energy CV ($G_f$) influences the brittleness number $s$

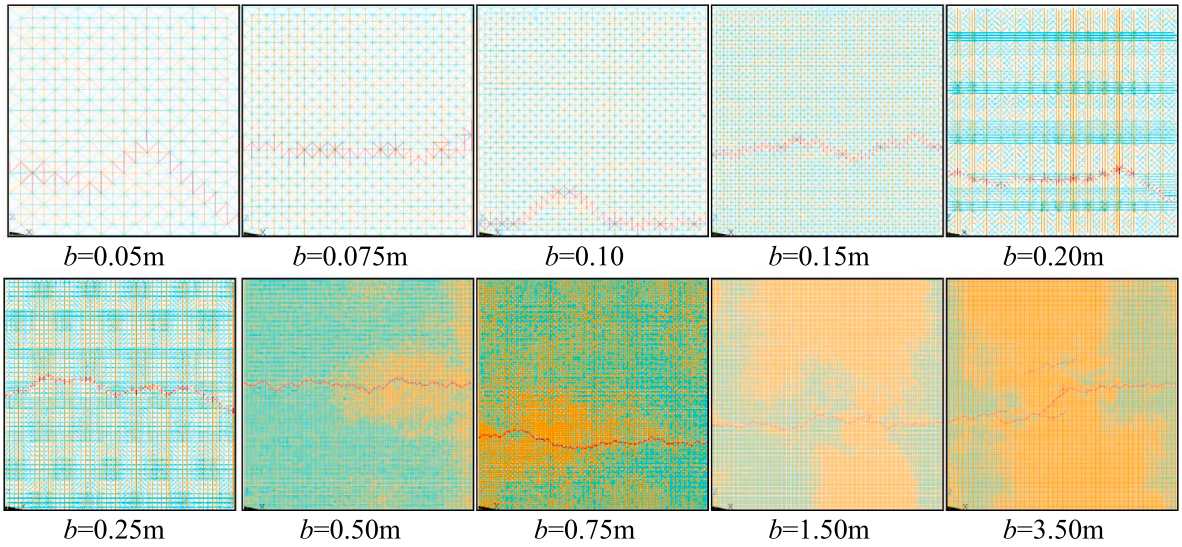


**Fig. 5.** Damage distribution and rupture configuration of specimens of various sizes subjected to applied displacements inducing uniaxial tension. The characteristic specimen size b varies between 0.05 m and 3.5 m. The broken bars are indicated in red, the damaged bars in orange and the undamaged bars in cyan.

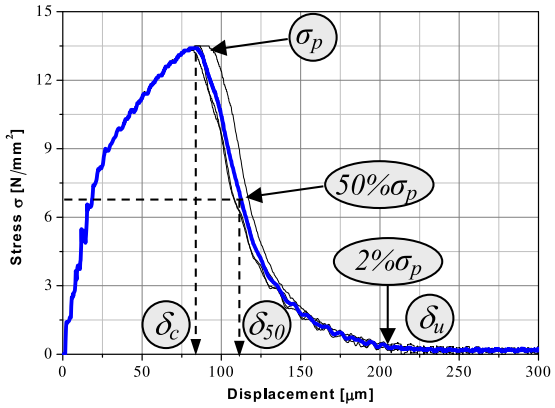


**Fig. 6.** Curves for the mean vertical stress at lower support versus mean displacement for the b = 0.20 m rock specimen obtained from four simulations (black) and the average curve ones (blue).

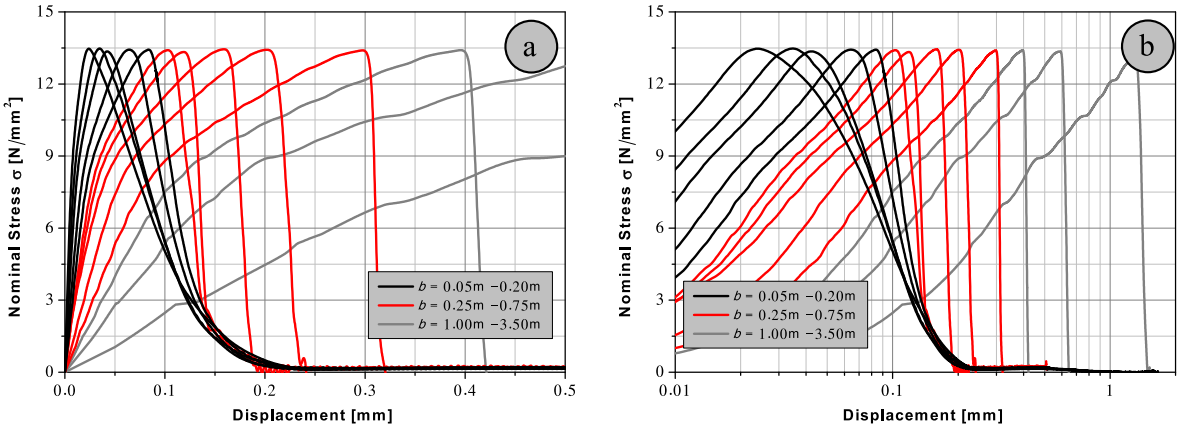


**Fig. 7.** (a) Displacement versus stress and (b) log displacement versus stress curves for different size specimens. Ductile behavior when b < 0.25 (black curves), brittle behavior when b > 0.75 m (gray curves), transition ductile-to- brittle behavior when b belongs to the interval [0.25, 0.75] (red curves).

**Table 7**
Mean values of peak stress, critical and rupture displacement of different simulated specimen size.

| $b$[mm] | $\sigma_p$[MPa] | CV[%] | $\delta_c$[μm] | CV[%] | $\delta_u$[μm] | CV[%] | $\delta_{50}$[μm] | $s$ Eq. (1) | $s_{LDEM}$ Eq. (14) |
|---|---|---|---|---|---|---|---|---|---|
| 50 | 13.461 | 1.10 | 26 | 7.42 | 225 | 4.53 | 93 | 3.26 | 5.41 |
| 75 | 13.518 | 0.85 | 34 | 7.30 | 211 | 5.01 | 89 | 2.67 | 4.42 |
| 100 | 13.415 | 0.98 | 43 | 5.63 | 207 | 4.08 | 94 | 2.33 | 3.83 |
| 150 | 13.508 | 0.63 | 64 | 0.04 | 213 | 0.14 | 103 | 1.90 | 3.12 |
| 200 | 13.473 | 0.39 | 85 | 3.13 | 213 | 2.44 | 110 | 1.64 | 2.71 |
| 250 | 13.429 | 0.68 | 105 | 1.31 | 203 | 1.76 | 126 | 1.46 | 2.42 |
| 300 | 13.393 | 0.16 | 124 | 0.15 | 185 | 4.77 | 132 | 1.35 | 2.21 |
| 400 | 13.488 | 0.31 | 166 | 1.29 | 184 | 3.33 | 176 | 1.16 | 1.91 |
| 500 | 13.471 | 0.30 | 205 | 1.36 | 228 | 2.41 | 216 | 1.04 | 1.71 |
| 750 | 13.455 | 0.39 | 301 | 1.92 | 322 | 1.72 | 301 | 0.85 | 1.40 |
| 1000 | 13.420 | 0.20 | 397 | 1.24 | 420 | 1.20 | 397 | 0.74 | 1.21 |
| 1500 | 13.437 | 0.20 | 605 | 0.76 | 646 | 0.76 | 605 | 0.60 | 0.99 |
| 3500 | 13.347 | 0.21 | 1325 | 1.87 | 1444 | 0.60 | 1325 | 0.39 | 0.65 |

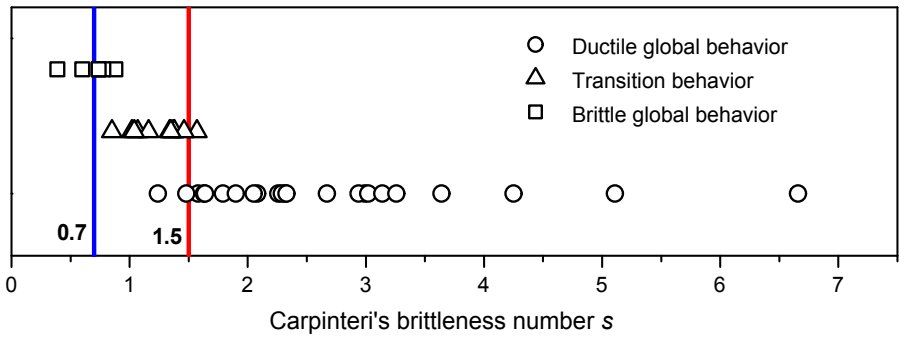


**Fig. 8.** Representation of the $s$ values in experimental and numerical results.

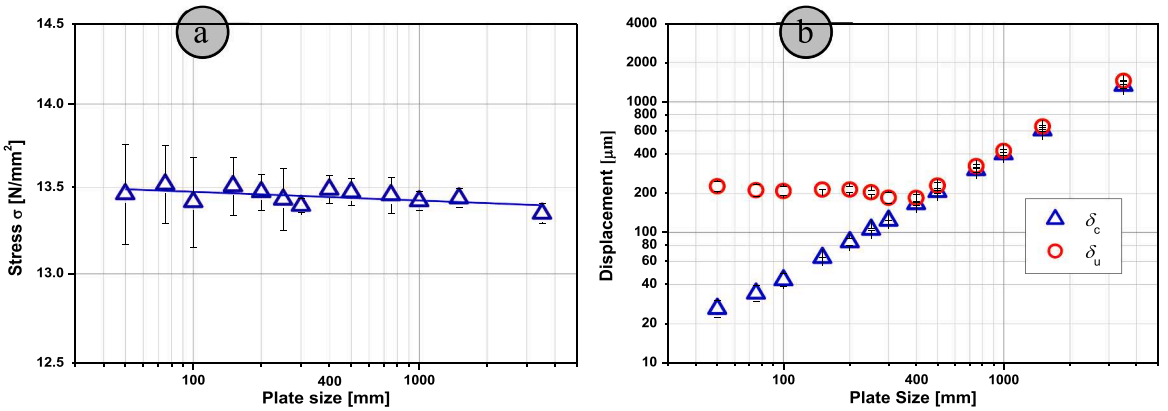


**Fig. 9.** (a) Ultimate global stress. (b) Ultimate and characteristic global displacement versus the specimen dimension. The mean values and bar with ± 2 standard deviation are indicated in the figure.

computed using the LDEM formulation. The simulations presented in section 4.1 were carried out using CV ($G_f$) = 40%, this value is usually employed to simulate quasi-brittle materials such as concrete and rocks (see e.g. [36,38]). Moreover, a particular study about the influence of the variability CV ($G_f$) was conducted in [30].

The white circle in Fig. 11, illustrates the LDEM simulations presented in the present paper. A set of simulations presented in Ref. [50] were also added in red, together with other results presented in Refs. [68,69] represented by gray circles.

In Fig. 11, it can be noticed that an approximate relationship between $s/s_{LDEM}$ could be considered independent of $d_{eq}/L$, if $d_{eq}/L > 100$ ($\varepsilon_r/\varepsilon_p \approx 60$). For lower values of this ratio, the level of the discretization influences the $s/s_{LDEM}$ result, finding responses in the interval [0.6, 1.5]. It is also important to notice that the influence of the fracture energy variation coefficient is significant.

When an element breaks, it generates a crack with a size related to its length, $L$. If this crack is smaller than the material equivalent length $d_{eq}$, it will not propagate until it reaches this critical dimension (after nucleation). If this crack size is closed to the material equivalent length $d_{eq}$, then it will propagate.

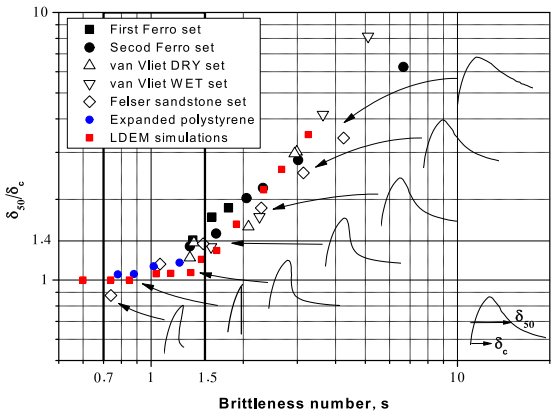


**Fig. 10.** Relation between the Carpinteri brittleness number, $s$, and the shape of the global stress - displacement curve.

A $s/s_{LDEM}$ greater than 1 indicates that the mean axial stress of all the LDEM elements ($\sigma_p^*$) is greater than the simulation maximum global stress ($\sigma_p$). This can be found with a more "brittle" constitutive model ($\varepsilon_r$ close to $\varepsilon_p$ or $d_{eq}$ close to $L$) and/or large dispersions in a random field. With a large dispersion, it is easier to find a less resistant element than the mean element resistance. When the element breaks, if the generated crack is of the size of $d_{eq}$, a brittle fracture occurs. In this case, the simulation's global response is close to the resistance of this first broken element, but much smaller than the mean resistance of all the other elements together.

Conversely, a $s/s_{LDEM}$ smaller than 1 indicates that the mean axial stress of all the LDEM elements ($\sigma_p^*$) is less than the simulation maximum global stress ($\sigma_p$). This occur when we have little dispersion of the random field (low CV) and/or a "ductile" constitutive model ($\varepsilon_r$ much larger than $\varepsilon_p$ or $d_{eq}$ bigger than $L$).

A practical application of the graphs presented in Fig. 10 to calibrate the LDEM model could be proposed:

1-. If experimental data about the material are available, together with the specimen size characterized by its $R$, the material properties $G_f$, $E$ and the stress versus displacement global curve, then the value of $s$ can be computed using the Eq. (1).
2-. Assuming that $s_{LDEM} = s$ using the Eq. (14), it is possible to obtain the material parameter $d_{eq}$.
3-. Adopting a level of discretization and the CV($G_f$) to be used in the simulation, it is possible to compute $d_{eq}/L$ and to obtain the ratio $s/s_{LDEM}$ using the plot presented in Fig. 11.
4-. With the corrected value of $s_{LDEM}$ and using Eq. (14), a better approximation of $d_{eq}$ could be computed.

Notice that $d_{eq}$ is a material parameter, and for this reason, if the model calibration is performed for one specimen, this value will not vary if the geometry and boundary conditions change.

In the present paper, a comparison between the global specimen behavior during damage process and the brittleness number is established. In [42,50,70] the link of the brittleness number with the dissipated energy and the final configurations obtained with LDEM simulations was also studied.

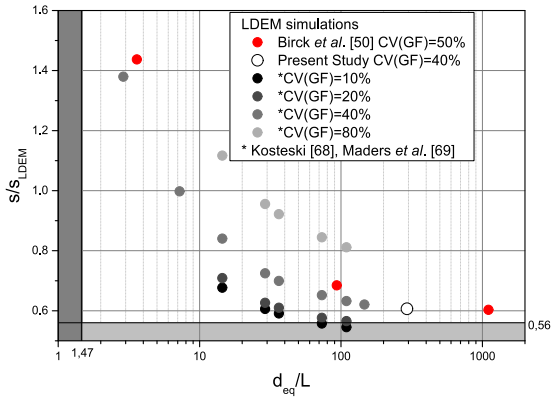


**Fig. 11.** Relation established between the global brittleness number and the brittleness number computed in the context of LDEM versus the ratio between the equivalent $d$ value over the element size used in the discretization.

## 5. Conclusions

In the present work, several sets of experimental and numerical results are reviewed with the aim to correlate the Carpinteri's brittleness number obtained to predict the global behavior (ductile, brittle, or ductile-to-brittle transitional behavior).

In all cases, the specimens were subjected to pure tensile stress and heterogeneous materials were also analyzed. Experimental results produced by other researchers or by the authors themselves are presented. No pre-cracked specimens were considered, that is, the spontaneous localization of the main crack was expected. The numerical approach used was a version of the Lattice Discrete Element Method that accounts for the random nature of the material employed. With this research work, it is possible to conclude that:

- A correlation between the $s$ number and the aspect of the global force/stress versus displacement/strain curve is evident in all the evaluated cases. For this reason, the computation of $s$ allows to predict what kind of behavior is to be expected for each specimen.
- The values computed using experimental and numerical results allow to perceive that for the boundary conditions used, when $s < 0.7$ is used as a lower bound, a global brittle behavior is expected. On the other hand, if $s > 1.5$, a ductile behavior is expected, moreover, in the interval of $s$ [0.7, 1.5], a ductile-to-brittle transitional behavior occurs. The extension of the present study to verify the influence of the boundary condition and the specimen geometry will be the focus of future works.
- The relationship between the traditional definition of $s$ and the definition of the brittleness number computed in the context of the numerical method used, $s_{LDEM}$, was presented. This relationship can be used to calibrate, in a consistent way, the LDEM method employed. It is possible to extend this methodology of calibration to other versions of the discrete element method (for example in Perydinamics), where spontaneous fracture can be also simulated.
- The satisfactory correlation between experimental and LDEM results confirms the robustness of this method as a numerical tool to model fracture processes in quasi-brittle materials.

## Declaration of Competing Interest

The authors declare that they have no known competing financial interests or personal relationships that could have appeared to influence the work reported in this paper.

## Acknowledgements

The present study was conducted with the financial support of the National Council for Scientific and Technological Development (CNPq) and the Coordination for the Improvement of Higher Level of Education Personnel (CAPES). Furthermore, we hope for future collaborations to take place and be agreed upon within and for a common Project between UNIPAMPA, Alegrete, and UFRGS, Porto Alegre, RS, Brazil, and Politecnico di Torino, Italy, for the Horizon 2020 Work Program "Nanotechnologies, Advanced Materials, Biotechnology, and Advanced Manufacturing and Processing".

## References

[1] Dugdale DS. Yielding of steel sheets containing slits. J Mech Phys Solids 1960;8(2):100–4. https://doi.org/10.1016/0022-5096(60)90013-2.
[2] Boyle RW, Sullivan AM, Krafft JM. Determination of plane strain fracture toughness with sharply notched sheets. Weld J Res Suppl 1962;41:428–32.
[3] Brown Jr WF, Srawley JE. Plane strain crack toughness testing of high strength metallic materials. No. 410, ASTM, Philadelphia, Pa: ASTM Special Technical publication; 1966.
[4] Mpalaskas AC, Matikas TE, Van Hemelrijck D, Papakitsos GS, Aggelis DG. Acoustic emission monitoring of granite under bending and shear loading. Arch Civ Mech Eng 2016;16(3):313–24. https://doi.org/10.1016/j.acme.2016.01.006.
[5] Mpalaskas AC, Thanasia OV, Matikas TE, Aggelis DG. Mechanical and fracture behavior of cement-based materials characterized by combined elastic wave approaches. Constr Build Mater 2014;50:649–56. https://doi.org/10.1016/j.conbuildmat.2013.10.022.
[6] Carpinteri A. Static and energetic fracture parameters for rocks and concretes. Mat Constr 1981;14(81):151–62. https://doi.org/10.1007/BF02473919.
[7] Carpinteri A. Application of fracture mechanics to concrete structures. J Struct Div (ASCE) 1982;108(4):833–48.
[8] Carpinteri A. Post-peak and post-bifurcation analysis of cohesive crack propagation. Eng Fract Mech 1989;32(2):265–78. https://doi.org/10.1016/0013-7944(89)90299-3.
[9] Carpinteri A. Cusp catastrophe interpretation of fracture instability. J Mech Phys Solids 1989;37(5):567–82. https://doi.org/10.1016/0022-5096(89)90029-X.
[10] Carpinteri A, Marenga C, Savadori A. Ductile-brittle transition by varying structural size. Eng Fract Mech 1985;21:263–71. https://doi.org/10.1016/0013-7944(85)90015-3.
[11] Carpinteri A. Scaling laws and renormalization groups for strength and toughness of disordered materials. Int J Solids Struct 1994;31(3):291–302. https://doi.org/10.1016/0020-7683(94)90107-4.
[12] Carpinteri A, Marega C, Savadori A. Size effects and ductile-brittle transition of polypropylene. J Mater Sci 1986;21:4173–8. https://doi.org/10.1007/BF01106526.
[13] Carpinteri A, Cornetti P, Barpi F, Valente S. Cohesive crack model description of ductile to brittle size-scale transition: dimensional analysis vs. renormalization group theory. Eng Fract Mech 2003;70:1809–39. https://doi.org/10.1016/S0013-7944(03)00126-7.
[14] Brincker R, Henriksen MS, Christensen FA, Heshe G. Size Effects on the Bending Behaviour of Reinforced Concrete Beams. Eur Struct Integr Soc 1999;24:127–37. https://doi.org/10.1016/S1566-1369(99)80064-8.
[15] Gao H. Application of fracture mechanics concepts to hierarchical biomechanics of bone and bone-like materials. Int J Fract 2006;138:101–37. https://doi.org/10.1007/s10704-006-7156-4.
[16] Corrado M, Cadamuro E, Carpinteri A. Dimensional analysis approach to study snap back-to-softening-to-ductile transitions in lightly reinforced quasi-brittle materials. A Int J Fract 2011;172(1):53–63. https://doi.org/10.1007/s10704-011-9646-2.
[17] Krajcinovic D. Damage mechanics. Amsterdam: Elsevier; 1986.
[18] Seleson P, Beneddine S, Prudhomme S. A force-based coupling scheme for peridynamics and classical elasticity. Comp Mat Sci 2013;66:34–49. https://doi.org/

10.1016/j.commatsci.2012.05.016.
[19] Silling SA. Reformulation of elasticity theory for discontinuities and long-range forces. J Mech Phys Solids 2000;48:175–209. https://doi.org/10.1016/S0022-5096(99)00029-0.
[20] Schlangen E, van Mier JGM. Crack propagation in sandstone: Combined experimental and numerical approach. Rock Mech Rock Engng 1995;28:93–110. https://doi.org/10.1007/BF01020063.
[21] Krajcinovic D, Vujosevic M. Strain localization-short to long correlation length transition. Int J Solids Struct 1998;35:31–2. https://doi.org/10.1016/S0020-9683(97)00307-7.
[22] Sagar RV, Raghu Prasad BK. Modeling heterogeneity of concrete using 2D lattice network for concrete fracture and comparison with AE study. Sadhana 2009;34:865–86. https://doi.org/10.1007/s12046-009-0052-7.
[23] Nagy E, Landis EN, Davids WG. Acoustic emission measurements and lattice simulations of microfracture events in spruce. Holzforschung 2010;64:455–61. https://doi.org/10.1515/hf.2010.088.
[24] Rinaldi A. Advances in Statistical Damage Mechanics (SDM): New Modeling Strategies. In Damage Mechanics and Micromechanics of Localized Fracture Phenomena in Inelastic Solids. CISM Courses and Lectures, vol. 525. Vienna: Springer; 2011.
[25] Mastilovic S, Rinaldi A. Two-Dimensional Discrete Damage Models: Discrete Element Methods, Particle Models, and Fractal Theories. In: Voyiadjis G, editor. Handbook of Damage Mechanics. New York, NY: Springer; 2015. p. 273–303.
[26] Riera JD. Local effects in impact problems on concrete structures. Proceedings of the Conference on Structural Analysis and Design of Nuclear Power Plants, vol. 3, Porto Alegre, October 3–5; 1984.
[27] Riera JD, Iturrioz I. Discrete element dynamic response of elastoplastic shells subjected to impulsive loading. Commun Numer Meth En 1995;11:417–26. https://doi.org/10.1002/cnm.1640110506.
[28] Riera JD, Iturrioz I. Discrete element model for evaluating impact and impulsive response of reinforced concrete plates and shells subjected to impulsive loading. Nucl Eng Des 1998;179:135–44. https://doi.org/10.1016/S0029-5493(97)00270-7.
[29] Kosteski LE, Riera JD, Iturrioz I, Singh RK, Kant T. Analysis of reinforced concrete plates subjected to impact employing the truss-like discrete element method. Fatigue Fract Eng M 2015;38:276–89. https://doi.org/10.1111/ffe.12227.
[30] Kosteski LE, Iturrioz I, Cisilino AP, Barrios D'ambra R, Pettarin V, Fasce L, Frontini P. A lattice discrete element method to model the falling-weight impact test of PMMA specimens. Int J Impact Eng 2016;87:120–31. https://doi.org/10.1016/j.ijimpeng.2015.06.011.
[31] Schnaid F, Spinelli L, Iturrioz I, Rocha M. Fracture mechanics in ground improvement design. Ground Improv 2004;8:7–15. https://doi.org/10.1680/grim.2004.8.1.7.
[32] Dalguer LA, Irikura K, Riera JD, Chiu HC. The importance of the dynamic source effects on strong ground motion during the 1999 Chi-Chi, Taiwan, Earthquake: Brief Interpretation of the Damage Distribution on Buildings. Bull Seismol Soc Am 2001;91(5):1112–27. https://doi.org/10.1785/0120000705.
[33] Dalguer LA, Irikura K, Riera JD. Simulation of tensile crack generation by three-dimensional dynamic shear rupture propagation during an earthquake. J Geophys Res 2003;108(B3):2144. https://doi.org/10.1029/2001JB001738.
[34] Iturrioz I, Birck G, Riera JD. Numerical DEM simulation of the evolution of damage and AE preceding failure of structural components. Eng Fract Mech 2019;210:247–56. https://doi.org/10.1016/j.engfracmech.2018.02.023.
[35] Birck G, Riera JD, Iturrioz I. Numerical DEM simulation of AE in plate fracture and analogy with the frequency of seismic events in SCRs. Eng Fail Anal 2018;93:214–23. https://doi.org/10.1016/j.engfailanal.2018.06.024.
[36] Rios RD, Riera JD. Size effects in the analysis of reinforced concrete structures. Eng Struc 2004;26:1115–25. https://doi.org/10.1016/j.engstruct.2004.03.012.
[37] Iturrioz I, Morquio A, Bittencourt E, Rosito áAvila V. Performance of the Discrete Element Method to represent the scale effect. Published in Mechanics of Solids in Brazil 2007, Brazilian Society of Mechanical Sciences and Engineering; 2007, p. 247–63.
[38] Iturrioz I, Miguel LFF, Riera JD. Dynamic fracture analysis of concrete or rock plates by means of the Discrete Element Method. Lat Am J Solids Stru 2009;6:229–45.
[39] Iturrioz I, Riera JD, Miguel LFF, Kosteski LE. Scale Effects in Quasi-Fragile Materials Subjected to Compress. IASMiRT, SMiRT 21 - New Delhi, India. November 6–11; 2011.
[40] Miguel LFF, Riera JD, Iturrioz I. Influence of size on the constitutive equations of concrete or rock dowels. Int J Numer Anal Meth Geomech 2008;32:1857–81. https://doi.org/10.1002/nag.699.
[41] Miguel LFF, Iturrioz I, Riera JD. Size effects and mesh independence in dynamic fracture analysis of brittle materials. CMES 2010;56:1–16. https://doi.org/10.3970/cmes.2010.056.001.
[42] Colpo AB, Kosteski LE, Iturrioz I. The size effect in quasi-brittle materials: Experimental and numerical analysis. Int J Dam Mech 2017;26:395–416. https://doi.org/10.1177/1056789516671776.
[43] Kosteski LE, Barrios D'Ambra R, Iturrioz I. Determinación de parámetros fractomecánicos estáticos y dinámicos utilizando el método de los elementos discretos compuestos por barras. Rev int métodos numér cálc diseño ing 2008;24(4):323–43https://www.scipedia.com/public/Kosteski_et_al_2008a.
[44] Kosteski LE, Barrios D'Ambra R, Iturrioz I. Fractomechanics parameter calculus using the Discrete Element Method. Lat Am J Solids Stru 2010;6:301–21.
[45] Kosteski LE, Iturrioz I, Batista RG, Cisilino AP. The truss-like discrete element method in fracture and damage mechanics. Eng Computations 2011;28:765–87. https://doi.org/10.1108/02644401111154664.
[46] Kosteski LE, Barrios D'Ambra R, Iturrioz I. Crack propagation in elastic solids using the truss-like discrete element method. I Int J Fract 2012;174:139–61. https://doi.org/10.1007/s10704-012-9684-4.
[47] Riera JD, Miguel LFF, Iturrioz I. Strength of Brittle Materials under high strain rates in DEM simulations. CMES 2011;82:113–36. https://doi.org/10.3970/cmes.2011.082.113.
[48] Iturrioz I, Lacidogna G, Carpinteri A. Experimental analysis and truss-like discrete element model simulation of concrete specimens under uniaxial compression. Eng Fract Mech 2013;110:81–98. https://doi.org/10.1016/j.engfracmech.2013.07.011.
[49] Iturrioz I, Lacidogna G, Carpinteri A. Acoustic emission detection in concrete specimens: Experimental analysis and lattice model simulations. Int J Dam Mech 2014;23:327–58. https://doi.org/10.1177/1056789513494232.
[50] Birck G, Iturrioz I, Lacidogna G, Carpinteri A. Damage process in heterogeneous materials analyzed by a lattice model simulation. Eng Fail Anal 2016;70:157–76. https://doi.org/10.1016/j.engfailanal.2016.08.004.
[51] Da Silva GS, Kosteski LE, Iturrioz I. Analysis of the failure process by using the Lattice Discrete Element Method in the Abaqus environment. Theor Appl Fract Mech 2020;107:102563https://doi.org/10.1016/j.tafmec.2020.102563.
[52] Nayfeh AH, Hefzy MS. Continuum modeling of three-dimensional truss-like space structures. AIAA Journal 1978;16:779–87. https://doi.org/10.2514/3.7581.
[53] Rinaldi A, Krajcinovic D, Peralta P, Lai YC. Lattice models of polycrystalline microstructures: a quantitative approach. Mech Mater 2008;40:17–36. https://doi.org/10.1016/j.mechmat.2007.02.005.
[54] Rocha MM, Riera JD, Krutzik NJ. Extension of a model that aptly describes fracture of plain concrete to the impact analysis of reinforced concrete. In Int. Conf. and Structural Mechanics in Reactor Technology, SMiRT 11, Trans. vol. J., Tokyo, Japan; 1991.
[55] Hillerborg A. A model for fracture analysis. Cod LUTVDG/TV BM-3005; 1978, p. 1–8.
[56] Kupfer HB, Gerstle KH. Behavior of concrete under biaxial stresses. J Eng Mech Div 1973;99(4):853–66.
[57] Kanninen MF, Popelar CH. Advanced fracture mechanics. Oxford University Press; 1985.
[58] Silling SA, Epton M, Weckner O, Xu J, Askari E. Peridynamic States and Constitutive Modeling. J Elast 2007;88:151–84. https://doi.org/10.1007/s10659-007-9125-1.
[59] Taylor D. The Theory of Critical Distances: A New Perspective in Fracture Mechanics. Elsevier; 2007.
[60] Puglia VB, Kosteski LE, Riera JD, Iturrioz I. Random field generation of the material properties in the lattice discrete element method. J Strain Anal Eng 2019;54(4):236–46. https://doi.org/10.1177/0309324719858849.
[61] Iturrioz I, Riera JD, Miguel LFF. Introduction of imperfections in the cubic mesh of the truss-like discrete element method. Fatigue Fract Eng M

2014;37(5):539–52. https://doi.org/10.1111/ffe.12135.
[62] Carpinteri A, Ferro G. Size effects on tensile fracture properties: A unified explanation based on disorder and fractality of concrete microstructure. Mater Struct 1994;27:563–71. https://doi.org/10.1007/BF02473124.
[63] Carpinteri A, Ferro G. Scaling behaviour and dual renormalization of experimental tensile softening responses. Mat Struct 1998;31:303–9. https://doi.org/10.1007/BF02480671.
[64] van Vliet MRA. Size effect in tensile fracture of concrete and rock. Ph.D. Thesis. Delft, The Netherlands: Delft University of Technology; 2000.
[65] van Vliet MRA, van Mier JGM. Size effects of concrete and sandstone. Heron 2000;45:91–108http://resolver.tudelft.nl/uuid:f2beb295-f41d-4db1-b126-8be73c23317b.
[66] Carpinteri A, Maradei F. Three-jack solution to obtain a truly stable and symmetric tensile concrete test. Exp Mech 1995;35:19–23. https://doi.org/10.1007/BF02325829.
[67] Birck G, Iturrioz I, Riera JD, Miguel LFF. Influence of mesh orientation in discrete element method simulations of fracture processes. J Strain Anal Eng Des 2018;53(6):400–7. https://doi.org/10.1177/0309324718775284.
[68] Kosteski LE. Aplicação do Método dos Elementos Discretos formado por barras no estudo do colapso de estruturas. Doctoral Thesis, Universidade Federal de Rio Grande do Sul, Porto Alegre; 2012 [in Portuguese]. http://hdl.handle.net/10183/56589.
[69] Maders L, Kosteski LE, Iturrioz I. Estudo do efeito de escala no método dos elementos discretos formado por barras. In Mecom 2012, Salta, Argentina. Mecánica Computacional, vol. XXXI, p. 1857–1876.
[70] Birck G, Rinaldi A, Iturrioz I. The fracture process in quasi-brittle materials simulated using a lattice dynamical model. Fatigue Fract Eng Mater Struct 2019;42(12):2709–24. https://doi.org/10.1111/ffe.13094.